

The Influence of Intermittent Localized Corrosion on the Mechanical Properties of Steel Rebars

Christian Paglia

Institute of Materials and Construction, University of Applied Sciences of Southern Switzerland, DACD, V. F. Ruchat 15, 6850 Mendrisio, Switzerland.

Corresponding author*Christian Paglia,**

Institute of Materials and Construction, University of Applied Sciences of Southern Switzerland, DACD, V. F. Ruchat 15, 6850 Mendrisio, Switzerland.

ORCID : <https://www.researchgate.net/profile/C-Paglia>

Submitted : 10 Mar 2025 ; Published : 3 Apr 2025

Citation: Paglia, C. (2025). The Influence of Intermittent Localized Corrosion on the Mechanical Properties of Steel Rebars. *J mate poly sci*, 5(2) :1-8. DOI : <https://doi.org/10.47485/2832-9384.1072>

Abstract

Steel rebars are conventionally used in combination with concrete in buildings and civil engineering structures. A main degradation issue of these composite systems is the localized corrosion of the steel rebars. This fact promotes a scaling of the concrete surface and an aggressive localized attack of the rebars, until a cross-section reduction and detrimental static consequences. In this concern, steel rebars were immersed in a 3.5 % weight NaCl solution. A set of rebars were subjected to continuous immersion in the solution, whereas another set to a cyclic exposure consisting of immersion and drying at 25°C, 50°C and 100°C. The cyclic exposure and the temperature influenced the corrosion speed. A different extent of localized deterioration was detected. Some surface corrosion features barely affected the tensile properties of the rebar. Only at a later corrosion stage, the morphological features of the degradation contributed to a lowering of the mechanical properties, especially the tensile strength. The load-extension response of reinforcement during the tension tests did not directly correlate with the rust grade and the visual degradation aspect. An increase in the temperature and the water evaporation enhanced the presence of pits until 50°C. Corrosion pits were also seen, if the exposition to the solution was done in an intermittent rapid and cyclic mode, along the corroded bars. The corrosion features tend to affect the stress-strain response in tension of the rebars.

Keywords: Steel rebar, Intermittent localized corrosion, Tensile strength.

Introduction

The corrosion of steel rebar is a main concern in the building sector. The rebars mainly carries the tensile stress of reinforced concrete structures. The concrete cover provides a protection against the direct contact with the environmental degrading agents, such as rain, sun radiation, CO₂, pollutants and salts. However, with time and depending on the concrete cover quality, the detrimental agents enter the concrete and reach the steel rebars. The presence of chloride enhances the phenomena, by turning the degradation into a dangerous localized form. Steel rebars embedded within Portland cement-based systems are affected by this form of deterioration. Nonetheless, waste-based geopolymer systems behave similarly with respect to the steel rebar corrosion (Wasima et al., 2021). The combination of oxygen, water, chlorides from sea water or de-icing salts or the cyclic combination of these elements lead to cracking and spalling of the concrete cover (Torres-Acosta, 1999) and severe durability issues in reinforced concrete structures (Bazant, 1979). The lost of the load bearing capability is a major concern (Yao & Chen, 2022). Different methods (Bazant, 1979) try to assess the corrosion behaviour of the steel rebars embedded within concrete and the dishomogeneous corrosion

products distribution around the rebars. The chloride-induced form of corrosion is by far more intense than the carbonation-induced corrosion. The former exhibits an intense and localized attack, thus leading to the reduction of the steel rebar section in extreme cases. The formation of corrosion products with a higher volume as compared to the original steel, also leads to a mass and rebar-concrete adhesion loss, thus lowering the mechanical properties of the steel rebars (Sanchez et al., 2017). Pits depth and cross-sectional areas exhibit a relevant influence on the ultimate strength and strain also on strands (Franceschini et al., 2022).

The relationship between the mechanical properties, namely the stress-strain properties of the rebar, depending on the corrosion level, is a difficult task to be clarified. Generally, the mechanical properties and the ductility of the rebars are negatively affected by an increasing corrosion stage. Nonetheless, the measurements and identification of the corrosion level, the steel rebar type and the multiple detrimental actions may exhibit a controversial relationship between the steel rebar mechanical performance and the corrosion stage (Zhang et al., 2012; Apostolopoulos

et al., 2013; Zhu et al., 2017; Subramanian et al., 2018). On the one side, the reduction of the strain at maximum force seems more pronounced as compared to the ultimate strength reduction during corrosion progression (Tang et al., 2014). Impressed current (Sun et al., 2018) or real exposed reinforced concrete steel rebars (Fernandez & Berrocal, 2019) can be taken to verify the relation with the mechanical properties. On the other side, the corrosion of steel rebars is associated with an increase in the volume of the corrosion products. This is particularly seen with the carbonation-induced uniform corrosion. In this case, the internal stress causes cracking and concrete cover spalling along the rebars. On the other hand, the prediction of the corrosion process and stage based on the visible signs along the concrete cover surface may not be reliable. In fact, the formation of corrosion products for the chloride-induced corrosion may be delayed or even not present (Angst et al., 2012). However, the stress-strain curve may be correlated with the corrosion level. A premature yielding and a disappearing yielding plateau seem to be observed with an increasing localized corrosion stage, while localized pitting corrosion seems to exhibit a higher reduction of the strain at early stage as compared to extensive pitting corrosion at a later stage. Contrarily, the ultimate tensile strength related to the cross-sectional area, seems to show only a slight decrease with increasing corrosion stage (Chena et al., 2020).

The effect of the temperature on the corrosion of the steel rebars is often investigated for a high temperature fire exposure (Thongchom et al., 2023), or for steel rebars processed with special thermal treatments or cooling procedures (Lundberg, 2002). Contrarily, the effect of atmospheric exposition temperatures, ranging from room temperature 25°C, 50°C up to 100°C is rather poorly clarified. These temperatures are often cyclically present during conventional corrosion and degradation processes. Furthermore, during restoration works in practice, the visual inspection of the steel rebar corrosion degree is often used as main and unique evaluation criteria to identify the conservation state and the repair actions to be considered. In fact, the visual aspect of the rebars, the type of corrosion, the presence of pits, their frequency and the depth estimation are often taken as main evaluation points for the degradation. Nevertheless, it is difficult to estimate the influence of the corrosion stage on the mechanical properties of the rebar.

This work aims at supporting the visual evaluation of the corrosion stage along steel rebars in practice and its possible consequence on the tensile strength properties. In addition, the influence of the intermittent localized corrosion by cyclic water evaporation and 3.5% weight NaCl exposition and the temperature on the visual appearance of the corrosion morphology is also investigated with respect to the tensile properties of the rebars.

Experimental Procedure

The material used was a steel rebar B 500 C with a nominal diameter of 12 mm. The chemical analysis exhibits a Carbon content of 0.20%, a Phosphorous content of 0.023%, a

Sulphur content of 0.040%, a Copper content of 0.39% a Nitrogen content of 0.010% and a Carbon a equivalent Ceq of 0.35, which makes the steel weldable. The main mechanical properties reported on the technical specification were a yield strength Re of 524 Mpa, a tensile strength Rm of 617 Mpa, a ratio Rm/Re of 1.18 and a strain Agt of 11.4 %. The main material requirement classes are indicated below (Table 1).

Steel rebar	B500A	B500B	B500C
Ductility class	A	B	C
Yield strength f_{yk} [N/mm ²] ²⁽³⁾	500	500	500
Ratio $(R_m/R_e)_k$	$\geq 1.05^{(4)}$	≥ 1.08	≥ 1.15 ≤ 1.35
Strain A_{gt} [%]	$\geq 2.5^{(4)}$	≥ 5.0	≥ 7.5

Table 1: Steel rebar classes (Swiss standard SIA 262:2003 Civil Engineering, Concrete Structures, 2003).

A visual and optical inspection were done, while for the fractographic analysis, a scanning electron microscopy with an applied voltage of 15 KV was used. The tensile strength of the steel rebars with the evaluation of the mean mechanical parameters was determined (Standard ISO 15630-1:2019, *Steel for the reinforcement and prestressing of concrete — Test methods, Part 1: Reinforcing bars, rods and wire, 2019*; Standard ISO 6892-1:2019, *Metallic materials — Tensile testing — Part 1: Method of test at room temperature, 2019*).

The steel rebars (3 sample for each condition) were exposed to the following conditions prior to the determination of the tensile strength:

- Rebars not exposed to NaCl solution, stored at 25oC
- Rebars continuously immersed in a 3.5 % weight NaCl solution at 25oC
- Rebars intermittently sprayed (every six weeks) with a constant amount of 3.5% weight NaCl solution and after two minutes placed in an oven at 50oC. Procedure repeated for 10 months.
- Rebars intermittently sprayed (every six weeks) with a constant amount of 3.5% weight NaCl solution and after two minutes placed in an oven at 100oC. Procedure repeated for 10 months.

The rust grade was determined by analyzing the visual appearance of the rebar's surface, after exposition to the NaCl solution and to the temperatures and by determining the rust grade. The following scala with an increasing corrosion stage was applied (Standard ISO 8501-1:2007, *Preparation of steel substrates before application of paints and related products — Visual assessment of surface cleanliness — Part 1: Rust grades and preparation grades of uncoated steel substrates and of steel substrates after overall removal of previous coatings, 2007*):

Rust grade A: steel surface covered with scale, but little rust.

Rust grade B: steel surface begins to rust and scale start to flake.

Rust grade C: steel surface rusted and the rust can be scraped. Slight pitting visible.

Rust grade D: steel surface rusted away and general pitting is visible.

Results and Discussion

The visual appearance of the steel rebars after the exposition to the NaCl solution and to the temperatures exhibits variable

degree of corrosion. The reference specimens do not exhibit a visual presence of uniform corrosion or pits (Fig. 1 left). The steel rebars exposed at 25°C exhibit a rust grade D, namely the highest presence of corrosion features (Fig. 1 centre-left). By increasing the temperature, the rust grade shifts from the level C, for the specimens heated at 50°C (Fig. 1 centre-right), to the level B for the specimens exposed to a temperature of 100°C (Fig. 1 right).



Figure 1: Steel rebars exposed to a 3.5% wt. NaCl solution and after the exposition to an increasing temperature (from left to right).

A more detail investigation of the corrosion features along the steel rebar surface indicates the reference samples with a relatively clean surface (Fig. 2 left). Contrarily, the samples exposed at 25°C exhibit a more advanced corrosion stage (Fig. 2 centre-left), although a more intense localized form is seen for the samples exposed at 50°C (Fig. 2 centre-right), followed by the 100°C exposed samples. In this latter case, the water evaporation is faster and the corrosion intensity is slightly reduced (Fig. 2 right).

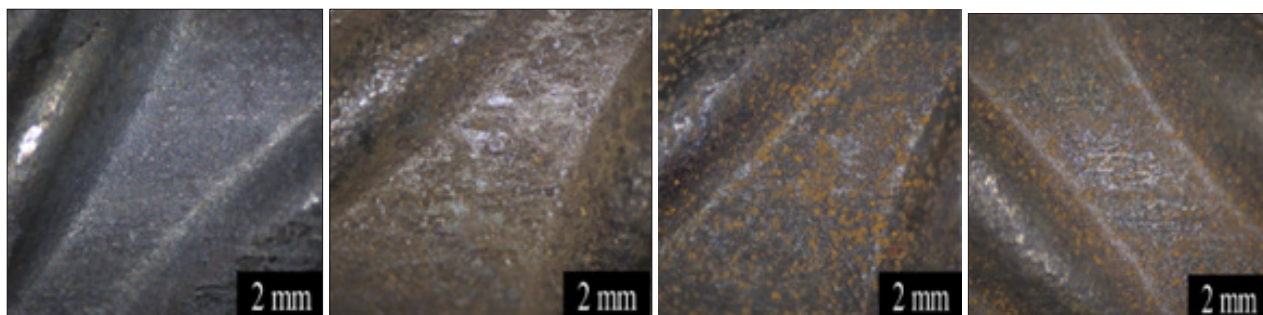


Figure 2: Binocular lens images of the corrosion morphology along the steel rebars: reference, rebar at 25°C, rebar at 50°C, rebar at 100°C (from left to right).

The stress-strain curves shape of the reference specimens exhibits a yield plateau and a yield strength $R_{p0.2} / R_e$ of 670 ± 16 MPa. The maximum tensile strength reaches 772 ± 23 MPa and the strain A_{gt} shows a mean value of $12 \pm 1.5\%$ (Fig. 3). A slight strain hardening and necking in the final phase of the curves are observed.



Figure 3: Stress (y-axis)-strain (x-axis) curves shape of the reference steel rebars.

The graphs of the steel rebar specimens continuously exposed to the 3.5 weight % NaCl and showing the highest rust grade D, indicate a rusted steel surface and with a general pitting and a clear yield plateau (Fig. 4). This in spite of the relatively advanced corrosion stage (Chena et al., 2020). The yield strength $R_{p0.2} / R_e$ exhibits a mean value of 573 ± 94 MPa. The maximum tensile

strength shows a value of 674 ± 94 Mpa and the strain A_{gt} shows $13 \pm 0.7\%$.

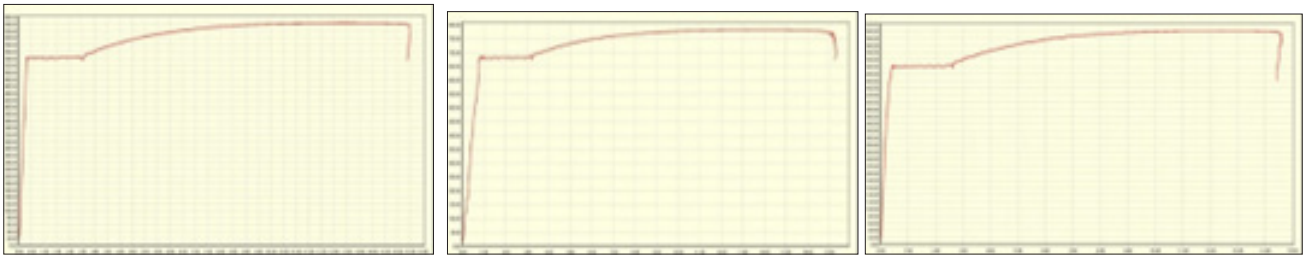


Figure 4: Stress (y-axis)-strain (x-axis) curves shape of the steel rebars continuously immersed in a 3.5 % NaCl at 25oC.

An increase in the temperature at 50oC for the specimens intermittently sprayed (every six weeks) with a constant amount of 3.5% NaCl solution and after two minutes placed in an oven at 50oC, with the procedure repeated for 10 months, maintains a characteristic shape of the stress-strain curves, with the mean yield strength $R_{p0.2} / R_e$ at 496 ± 2.5 MPa, the maximum tensile strength at 600 ± 0.5 MPa and the strain A_{gt} at 12.6 ± 0.4 % (Fig. 5).



Figure 5: Stress (y-axis)-strain (x-axis) curves shape of the steel rebars intermittently sprayed with a constant amount of 3.5% NaCl solution and after two minutes placed in an oven at 50°C.

The cyclic exposition to the 3.5% weight NaCl solution and the placing for two minutes at 100oC indicates a similar stress-strain curve shape with a yield strength $R_{p0.2} / R_e$ of 555 ± 96 MPa, the maximum tensile strength at 668 ± 117 MPa and the strain A_{gt} at $13 \pm 0.4\%$ (Fig. 6).



Figure 6: Stress (y-axis)-strain (x-axis) curves shape of the steel rebars intermittently sprayed with a constant amount of 3.5% NaCl solution and after two minutes placed in an oven at 100°C.

The curve shape of the samples exposed to different temperatures in the 3.5% weight NaCl solution shows a similar trend with the elastic region, the yield point, a plateau, a strain hardening region, the necking zone and the failure point.

However, as compared to the reference uncorroded samples, the corroded samples exhibit a lowering of the mechanical properties (Sanchez et al., 2017). The lowest values are seen for the 50oC exposed samples, that show a more intense localized corrosion phenomena. The 100oC exposed samples show less intense localized corrosion pits and may have a slight mechanical recovery, due to the temperature. The corrosion of the 25oC exposed samples is more homogeneously distributed, because of the lack of a significant water evaporation and chloride enrichments (Fig. 7).

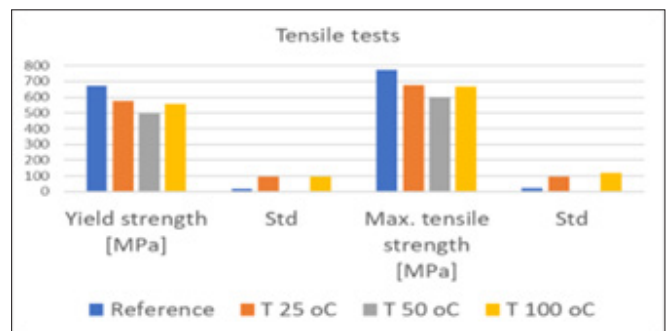


Figure 7: Mean yield strength and maximum tensile strength of the specimens treated with intermittent chloride and temperature exposure.

At 25°C, the corrosion of the samples immersed in the NaCl solution is clearly visible and a reduction of 15% of the yield strength and 13% of the maximum tensile strength are clearly observed. A similar behaviour of the mechanical properties is seen for the 100°C samples, while the 50°C exposed specimens exhibit an additional slight reduction of the mechanical properties, likely due to the more localized corrosion morphology and intense pitting formation. This temperature may accelerate the kinetics of the localized corrosion. However, the temperature is still not enough to cause a too rapid evaporation of the water as for the 100°C exposed samples. In this latter case, the pit formation is partially inhibited. The rust degree B, C and D decrease the mechanical properties and show a maximum variation of 90 Mpa of the tensile strength. Nevertheless, no direct correlation exists between the rust grade seen on the surface and the reduction of the properties (Zhang et al., 2012; Apostolopoulos et al., 2013; Zhu et al., 2017; Subramanian et al., 2018), as far as the corrosion stage remains in a low to medium level with a few craters and no relevant cross-sectional reduction is measured. This is due to the variable intensity of the localized aggressive spots. In addition, the temperature may largely regulate the corrosion process, speed and form. The pits agglomeration at 25°C emphasizes the advanced corrosion stage and the surface visual appearance of the samples as compared to the 50°C and 100°C samples. With a temperature of 50°C, the localized corrosion is accelerated, while for the 100°C exposed specimens, the rapid humidity decrease, due to higher temperature, lowers the intensity of the localized corrosion.

The modulus of elasticity is slightly related to the corrosion advancement stage and type. A more uniform distribution of corrosion pits with the 25°C treatment seems to reduce the values to a lower level as compared to the more localized pits presence of the 50°C exposition or for the specimens exposed to 100°C (Fig. 8).

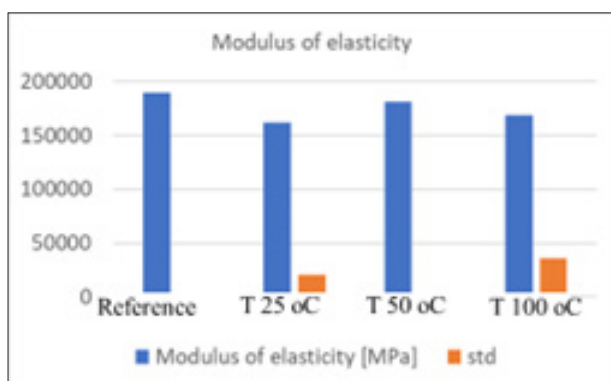


Figure 8: Modulus of elasticity of the steel rebars after the different exposure conditions and temperature. The standard deviations are not visible in the graph, when they are too small.

A slightly longer yielding plateau is seen for the corroded samples, especially for the 100°C treated specimens. However,

this behaviour is likely not influenced by the temperature exposition at 100°C. Nevertheless, the values do not change significantly for all tested samples (Fig. 9).

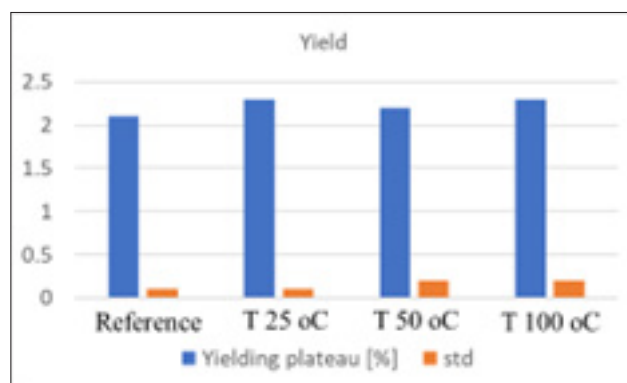


Figure 9: Range [%] of the yielding plateau in the stress-strain graphs of the steel rebars after the different exposure conditions and temperature. The standard deviations are indicated on the side of the columns.

The Agt strains appear not to clearly discriminate the influence of the corrosion on the deformation capability of the rebars. The values are relatively similar at all temperatures. In spite of the higher reduction of the strain as compared to the ultimate tensile strength with an advancement of the corrosion level (Chena et al., 2020), the corrosion stage variation between rust grades (A-D) seems to even slightly increase the ductility (Fig. 10). This is also seen for the highest rust grade D, where the steel rebar surface is completely rusted and general pitting is visible. On the other hand, the corrosion level did not reach yet the formation of relevant craters and cross section loss.

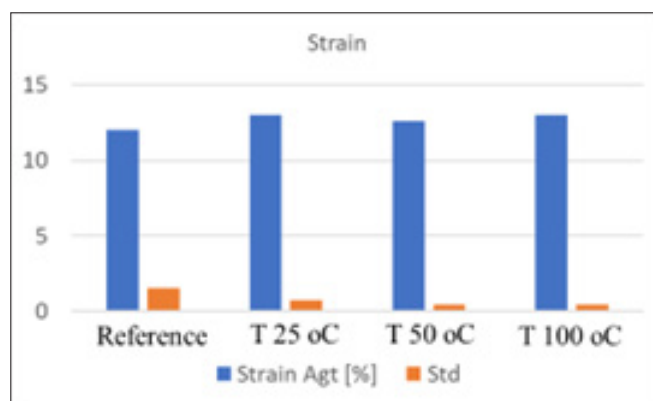


Figure 10: Strain Agt registered on the stress-strain graphs of the steel rebars after the different exposure conditions and temperature. The standard deviations are indicated on the side of the columns.

The fracture morphology exhibits a ductile fracture mode of the samples with cup and cone fracture as well as a clear necking in the deformation region (Fig. 11).

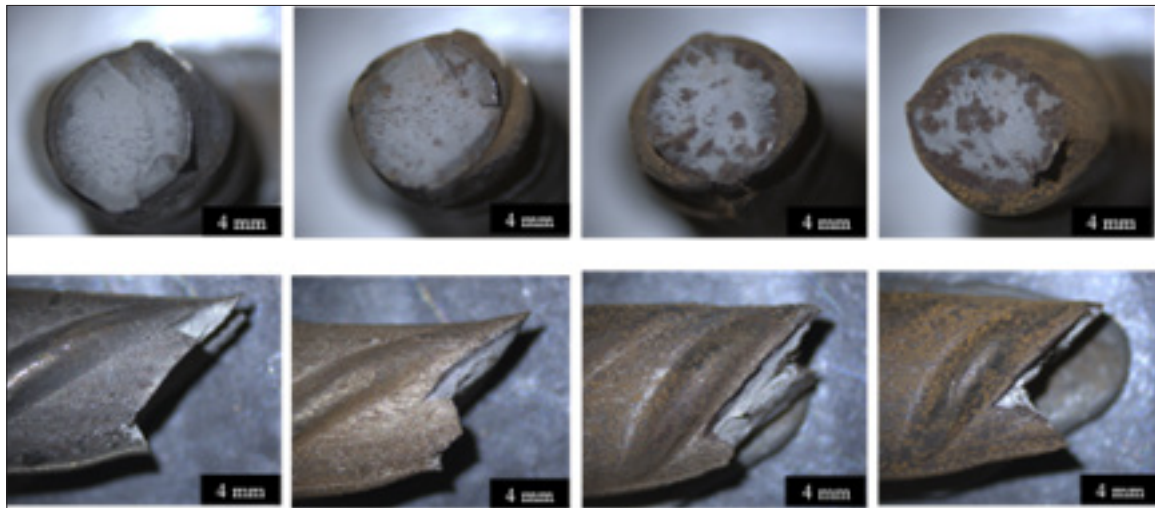


Figure 11: Fracture surface of the specimens for the reference, the sample treated at 25°C and constantly immersed in a NaCl 3.5% weight solution, the samples intermittently exposed to a NaCl 3.5% weight solution and treated at 50°C and the samples intermittently exposed to a NaCl 3.5% weight solution and treated at 100°C (from left to right).

The reference untreated and uncorroded specimens exhibit fine cracks and ductile dimples along the fracture surface (Fig. 12 left-right).

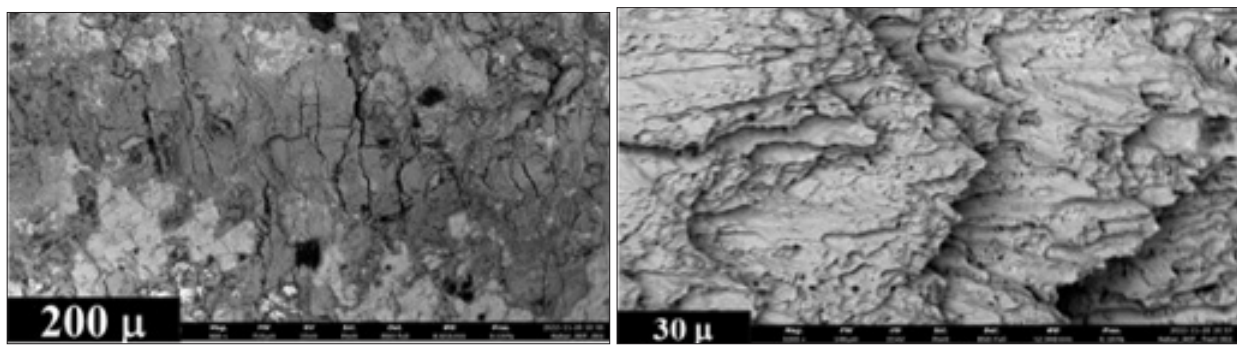


Figure 12: Fracture surface of the untreated reference steel rebars.

It is difficult to localize the initiation sites along the fracture surface of the steel rebars continuously exposed to the 3.5% weight solution at 25°C. Cracks and microcracks are present on the surface (Fig. 13 left). Surface corrosion products are partially visible (Fig. 13 centre), but the anodic dissolution features are not enough deep to clearly create identifiable corrosion sites for the cracking and the rupture initiation of the specimens. Such tensile tests performed at a relatively high speed rate as compared to environmentally assisted cracking, which are carried out at lower strain rates, are only partially influenced by the corrosion sites. The step-like and shear-tongue features as well as the ductile dimples (Fig. 13 right) indicate the general ductility of the specimens.

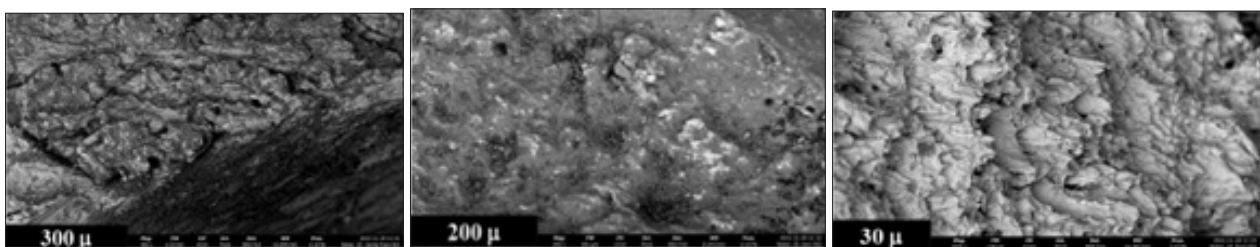


Figure 13: Fracture surface of the steel rebars continuously exposed to the 3.5% weight solution at 25°C.

More localized aggressive corrosion pits, due to water intermittent evaporation and sub-parallel cracks perpendicular to the tensile direction and occasionally mud-crack pattern are seen in the specimens treated at 50°C (Fig. 14).

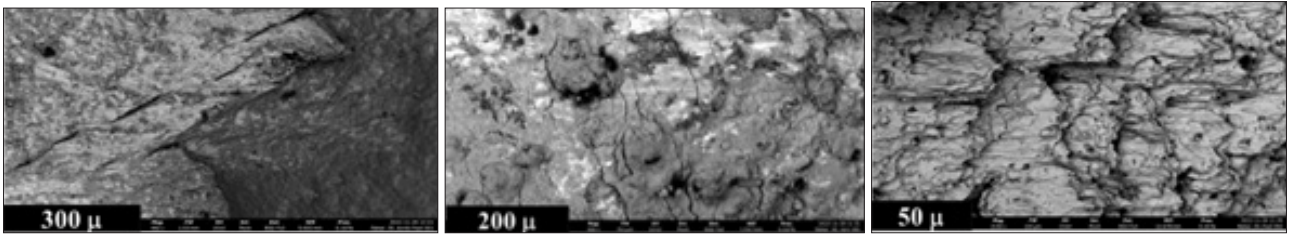


Figure 14: Fracture surface of the steel rebars intermittently sprayed with a constant amount of 3.5% NaCl solution and after two minutes placed in an oven at 50°C. Procedure repeated for 10 months.

In this case, the corrosion pits tend to create the initiation sites for cracking (Fig. 15 left), although no clear distinct zones are seen, due to high deformation rates. The specimens treated at 100°C exhibit less visible and intense corrosion pits (Fig. 15 centre) and slightly more shear deformation features can be observed along the fracture surface (Fig. 15 right).

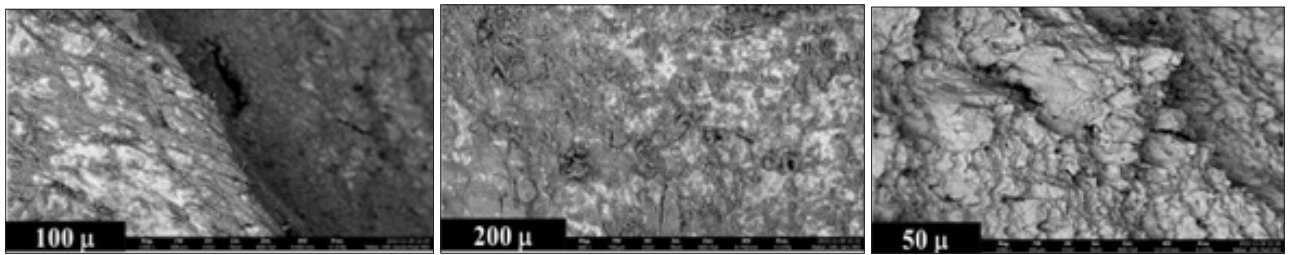


Figure 15: Fracture surface of the steel rebars intermittently sprayed with a constant amount of 3.5% NaCl solution and after two minutes placed in an oven at 100°C. Procedure repeated for 10 months.

Conclusions

The corrosion surface features and morphology along the rebars influence the mechanical properties of reinforcing steel rebars. The localized corrosion pits distributed along the steel surface slightly change the load-extension graph of reinforcement in tension tests. The yield strength, the ultimate strength, the modulus of elasticity and the strain to failure are slightly modified from the corrosion features. The mechanical properties and the corrosion morphology are not always directly correlated with the rust grade and the visual appearance, in the case of intermittent localized corrosion. However, the distribution of pits along the corroded bars, caused by the locally enhanced corrosion intensity, due to temperature increase and the water evaporation, especially at 50°C, even if only during an intermittent rapid and cyclic mode, may affect the stress-strain response in tension of the steel rebars.

Acknowledgments

The author would like to thank the technicians of the Institute of materials and construction, Supsi.

References

1. Wasima, M., Ngo, T. D., & Law, D. (2021). Durability performance of reinforced waste-based geopolymer foam concrete under exposure to various corrosive environments. *Case Studies Construction Materials*, 15(1). DOI: <https://doi.org/10.1016/j.cscm.2021.e00703>.
2. Torres-Acosta, A. A. (1999). Cracking Induced By Localized Corrosion of Reinforcement In Chloride Contaminated Concrete (Ph.D. dissertation). USA, Dept. of Civil and Environmental Engineering, University of South Florida.
3. Bazant, Z. P. (1979). Physical model for steel corrosion in sea structures –Theory. *(ASCE) J. Struct. Div.*, 105(6), 1137–1153. https://www.scielo.org.mx/scielo.php?pid=S2007-68352018000300317&script=sci_arttext_plus&tlng=en
4. Yao, J. & Chen, J. (2022). Sensitivity analysis of the deterioration of concrete strength in marine environment to multiple corrosive ions. *Front. Struct. Civ. Eng.*, 16, 175–190. DOI: <https://doi.org/10.1007/s11709-021-0791-z>
5. Bazant, Z. P. (1979). Physical model for steel corrosion in sea structures –applications. *J. Struct. Div. (ASCE)*, 105(6), 1155–1166. <https://doi.org/10.1061/JSDEAG.0005169>, <https://trid.trb.org/View/91558>
6. Sanchez, J., Fullera, J. & Andrade, C. (2017). Corrosion-induced brittle failure in reinforcing steel. *Theor. Appl. Fract. Mech.*, 92, 229–232. DOI: <https://doi.org/10.1016/j.tafmec.2017.08.006>
7. Franceschini, L., Vecchi, F., Tondolo, F., Belletti, B. & Sanchez Montero, J. (2022). Mechanical behaviour of corroded strands under chloride attack: A new constitutive law. *Construction and Building Materials*, 316, 125872. DOI: <https://doi.org/10.1016/j.conbuildmat.2021.125872>
8. Zhang, W., Song, X., Gu, X., & Li, S. (2012). Tensile and fatigue behavior of corroded rebars. *Construction Building Materials*, 34, 409–17. DOI: <http://dx.doi.org/10.1016/j.conbuildmat.2012.02.071>

9. Apostolopoulos, C. A., Demis, S., & Papadakis, V. G. (2013). Chloride-induced corrosion of steel reinforcement—Mechanical performance and pit depth analysis. *Construction Building Materials*, 38, 139–46. DOI:<http://dx.doi.org/10.1016/j.conbuildmat.2012.07.087>
10. Zhu, W., François, R., Poon, C. S., & Dai, J. G., (2017). Influences of corrosion degree and corrosion morphology on the ductility of steel reinforcement. *Construction Building Materials*, 148, 297–306. DOI:<http://dx.doi.org/10.1016/j.conbuildmat.2017.05.079>
11. Subramanian, S. J., Sharma, S., Rajagopal, R., & Pillai, R. G. (2018). Assessment of Stress-Strain Behavior of Corroded Steel Reinforcement Using Digital Image Correlation (DIC). *J. Test. Eval.*, 46, 1874–90. DOI: <https://doi.org/10.1520/JTE20160487>
12. Tang, F., Lin Z., Chen G., Yi W., (2014). Three-dimensional corrosion pit measurement and statistical mechanical degradation analysis of deformed steel bars subjected to accelerated corrosion. *Construction Building Materials*, 70, 104–17. DOI:<http://dx.doi.org/10.1016/j.conbuildmat.2014.08.001>
13. Sun, X., Kong, H., Wang, H., & Zhang, Z., (2018). Evaluation of corrosion characteristics and corrosion effects on the mechanical properties of reinforcing steel bars based on three-dimensional scanning. *Corrosion Science*, 142, 284–94. DOI:<http://dx.doi.org/10.1016/j.corsci.2018.07.030>
14. Fernandez, I., & Berrocal C. G., (2019). Mechanical properties of 30 year-old naturally corroded steel reinforcing bars. *Int. J. Concr. Struct. Mater.*, 13, 9. <https://ijcsm.springeropen.com/articles/10.1186/s40069-018-0308-x>
15. Angst, U., Elsener, B., Jamali, A., & Adey, B. (2012). Concrete cover cracking owing to reinforcement corrosion – theoretical considerations and practical experience. *Materials and corrosion*, 63(12). <https://doi.org/10.1002/maco.201206669>
16. Chena, E., Berrocala, C. G., Fernandez, I., Löfgrena, I., & Lundgren, K. (2020). Assessment of the mechanical behaviour of reinforcement bars with localised pitting corrosion by Digital Image Correlation. *Engineering structures*, 219, 110936. DOI: <http://dx.doi.org/10.1016/j.engstruct.2020.110936>
17. Thongchom, C., Kongwat, S., Jaitrong, J., Keawsawasvong, S., Van Hong Bui, L., Stitmannathum, B. & Mousa, S. (2023). Effect of Elevated Temperatures on Mechanical Properties of Spliced and Non-Spliced Steel Reinforcements: *Experimental Study. Buildings*, 13(6), 1419. <https://doi.org/10.3390/buildings13061419>.
18. Lundberg, S-E. (2002). Optimization of corrosion resistance and mechanical properties on quenched and tempered rebar. *Scandinavian Journal of Metallurgy*, 31(3), 234-240. DOI: <https://onlinelibrary.wiley.com/doi/10.1034/j.1600-0692.2002.310311.x>
19. Swiss standard SIA 262:2003. (2003). Civil Engineering, Concrete Structures, table 5.
20. Standard ISO 15630-1:2019. (2019). Steel for the reinforcement and prestressing of concrete — Test methods, Part 1: Reinforcing bars, rods and wire. <https://www.iso.org/standard/66130.html>
21. Standard ISO 6892-1:2019. (2019). Metallic materials — Tensile testing — Part 1: Method of test at room temperature. <https://www.iso.org/standard/78322.html>
22. Standard ISO 8501-1:2007. (2007). Preparation of steel substrates before application of paints and related products — Visual assessment of surface cleanliness — Part 1: Rust grades and preparation grades of uncoated steel substrates and of steel substrates after overall removal of previous coatings. <https://www.iso.org/standard/43426.html>

Copyright: ©2025 Paglia, C. This is an open-access article distributed under the terms of the Creative Commons Attribution License, which permits unrestricted use, distribution, and reproduction in any medium, provided the original author and source are credited.